Energy levels and intensity parameters of Ho^{3+} ions in $Y_3Al_5O_{12}$ and $Lu_3Al_5O_{12}$

Brian M. Walsh [1] , Gary W. Grew, Norman P. Barnes

NASA Langley Research Center, Hampton, VA 23681

Abstract

The energy levels of the trivalent lanthanide Ho^{3+} in $Y_3Al_5O_{12}$ (YAG) and $Lu_3Al_5O_{12}$ (LuAG) have been measured. The Stark split levels for the first nine Ho manifolds in these materials have been measured, and the results have been fit to a free ion plus crystal field Hamiltonian to generate a theoretical set of energy levels. Crystal field parameters were varied to determine the best fit between experimental and theoretical energy levels. The energy levels of Ho:LuAG are seen to be very similar to those in Ho:YAG. However, subtle changes resulting from replacing Y^{3+} with Lu^{3+} in the garnet crystal $Y_3Al_5O_{12}$ result in different transition wavelengths in LuAG. This has implications for Ho $^5I_7 \rightarrow {}^5I_8$ lasers operating at ~ 2.1 μm. Although the energy levels have been measured previously in Ho:YAG, they have not been measured in Ho:LuAG. A comparison of the energy levels in Ho:YAG measured here show some discrepancies with previous measurements. The consistency of the energy level placements between Ho:LuAG and Ho:YAG indicate that the earlier studies may have some errors in the assignments. Finally, a Judd-Ofelt analysis is performed on Ho:YAG and Ho:LuAG to determine the intensity parameters, and thus, the transition probabilities and branching ratios of the first eight excited manifolds.

PACS: 71.70 Ch; 76.30 Kg; 78.20 Bh
keywords: A. Optical Materials, D. crystal fields, D. luminescence

Email address: Brian.M.Walsh@nasa.gov (Brian M. Walsh).
[1] mailing address: NASA Langley Research Center, MS 468, Hampton, VA 23681
phone: 1-757-864-7112, fax: 1-757-864-8828,

1 Introduction

Tm sensitized Ho luminescence in various host materials continues to be of interest for achieving laser action in the Ho ion around 2 μm. The main interest in 2 μm lasers is for use as eye-safe sources in environmental studies to detect aerosols in the atmosphere and in aviation to to detect wind shear and wake vorticies[1,2]. There is also interest in 2 μm lasers as surgical devices in medical procedures[3,4].

The Tm:Ho doped host materials chosen for 2 μm lasers are usually $Y_3Al_5O_{12}$ (YAG) and $YLiF_4$ (YLF). However, higher 2 μm laser efficiency has been observed in Tm:Ho doped $Lu_3Al_5O_{12}$ (LuAG)[5] and $LuLiF_4$ (LuLF)[6]. Tm:Ho doped LuAG and LuLF were developed at NASA Langley Research Center as potential 2 μm laser materials[7,8] using a quantum mechanical model. Lasing at 2.1 μm in Tm:Ho:LuAG and 2.06 μm in Tm:Ho:LuLF were also demonstrated[5,6] at NASA Langley Research Center, and as previously stated, showed improved performance over Tm:Ho doped YAG and YLF, respectively. The reason for this is that the lower laser level is in the ground manifold, making its exact position critical to the laser threshold. For quasi-four-level lasers, that is, lasers which have a finite Boltzmann thermal population in the lower laser level, such as 2 μm Tm:Ho lasers, the crystal field splitting of the Ho $^5I_8$ ground manifold determines the lower laser level population. A larger lower laser manifold splitting is beneficial in reducing lower laser level thermal populations, which benefits population inversion.

In order to calculate the lower laser level population, the energy levels must be known. The energy levels are also of interest for determining potential laser wavelengths and evaluating potential energy transfer processes. The energy levels in Ho:YAG have been measured by Gruber et al.[11,12], however, the energy levels in Ho:LuAG have not been measured previously. So, an examination of the energy levels of Ho:LuAG, an isomorph of Ho:YAG, would seem to be of interest to researchers utilizing Ho^{3+} ions in LuAG. In addition, a re-examination of the energy levels of Ho:YAG has revealed some discrepancies with the earlier studies of Gruber et al. Self-consistency between the measured levels of Ho:YAG and Ho:LuAG presented here adds a certain degree of confidence to the measurements. The complexity of these measurements offers a cautionary tale in that the spectra can be interpreted differently with regards to temperature and concentration dependence, as well as refining the placements with the fitting procedure.

2 The host materials YAG and LuAG

Lutecium Aluminum Garnet, $Lu_3Al_5O_{12}$ (LuAG), is a garnet isostructure similar to Yttrium Aluminum Garnet,$Y_3Al_5O_{12}$ (YAG). These materials are oxide crystals with a cubic garnet structure (space group $O_h{}^{10} - Ia3d$, number 230). Rare earth ions introduced into YAG and LuAG replace the Yttrium (Y) and Lutecium (Lu) ions, respectively. The site symmetry of the Lu^{3+} sites in LuAG is D_2, the same as for Y^{3+} ions in YAG. This means that while the overall symmetry of the YAG and LuAG crystals is cubic, the symmetry at the site of the Y^{3+} and Lu^{3+} ions in these crystals is D_2, so called because there exists three mutually perpendicular 2-fold rotation axes. A 2-fold rotation axis is one in which a rotation of π in the plane perpendicular to this axis produces an invariant configuration. This seemingly technical detail is very important in determining selection rules for dipole-dipole transitions in laser crystals. The selection rule table for D_2 site symmetry is given in table 1.

The crystallographic directions in YAG and LuAG consist of three equivalent directions. Crystals that exhibit this property are called isotropic, and as such, have no polarization dependence. Trivalent lanthanide ions replace, substitutionally, Yttrium (Y^{3+}) ions in YAG and Lutecium (Lu^{3+}) ions in LuAG with only small changes in the lattice constants since the lanthanide ion Ho has nearly the same atomic radius. In fact, the effective ionic radii of Y^{3+} and Lu^{3+} are 101.9 pm and 97.7 pm, respectively. The effective ionic radius of Ho^{3+} is 101.5 pm. These numbers are taken from Shannon[9] for a coordination number of 8. It is clear that Ho^{3+} ions are almost the same size for the Y^{3+} ion in YAG, and oversized for the Lu^{3+} ion in LuAG.

The relative strength of the crystal field for materials with similar structure can be assessed by comparison of the lattice constants, which are governed by the size of the host ions acting as dopant sites for the lanthanide ions. The strength of the crystal field determines the spread in energy of the Stark levels of a manifold in a lanthanide ion. The larger the crystal field, the larger the spread in Stark split levels.

The lattice constants for YAG and LuAG have been measured. Since these crystals are isotropic, all directions are equivalent. The lattice constants have been measured to be 12.0075 Å for YAG and 11.9164 Å for LuAG in a recent publication by Kuwano et al.[10] The lattice constant for YAG is seen to be slightly larger than LuAG. In simple terms this implies that YAG has a slightly weaker crystal field than LuAG. It is, therefore, reasonable to expect the energy levels of lanthanide ions in YAG to extend, in general, over a slightly smaller wavelength range than LuAG. The crystal field strength can be thought to 'stretch' the energy levels out. The higher the crystal field, the higher the 'stretching' is. The physical reason for this, of course, is that a

tighter lattice gives rise to larger crystal fields and larger crystal fields enhance the Stark effect. This is a well known phenomenon. It is for this reason that fluorides like YLF and LuLF have a much smaller Stark splitting for lanthanide dopant ions than garnets such as YAG and LuAG. The result is that when Ho^{3+} ions are substituted into LuAG, they experience a stronger crystal field than in YAG. These subtle changes can lead to differences in the thermal populations of the upper and lower Ho laser levels, thus affecting laser performance.

3 Experimental energy levels

The energy levels for Ho:YAG have been published previously in two articles by Gruber et al.[11,12] The energy levels for Ho:LuAG have not been measured previously. The energy levels for the first 9 manifolds in Ho:LuAG have been measured and are presented in this article. The energy levels in Ho:YAG have also been measured for completeness and for comparison with the published results by Gruber et al. There is some discrepancy between the energy levels measured here for Ho:YAG and those reported by Gruber et al. The experimental energy levels of Ho:YAG and Ho:LuAG were measured from emission and absorption spectra at temperatures ranging from 8K to 295K. Samples of YAG and LuAG with Ho concentrations ranging from 0.5% to 10.0% were used for these temperature dependent measurements. Emission and absorption spectra at a range of temperatures are necessary to determine the energy level placement of the various Stark levels. Temperature dependent absorption spectra can aid in determining a great many energy levels of excited states, but temperature dependent emission spectra is crucial in determining the ground state energy levels. Having a range of Ho concentrations is also of benefit in resolving weak lines. A comparison of the emission and absorption measurements for various temperatures and concentrations is crucial in obtaining a complete set of energy levels. Even in the most careful analysis of the large quantity of experimental data necessary for such measurements, it is not possible to determine all the energy levels experimentally. Because it is not possible in most cases to find all the energy levels experimentally, due to weak transitions and overlapping transitions, an iterative least squares fitting procedure between the experimental levels that can be measured, and those generated from a suitable set of crystal field parameters is employed.

Before an energy level fitting procedure can be implemented, a sufficient number of energy levels must be obtained experimentally. It has been pointed out that it is not possible to obtain all energy levels experimentally for reasons stated previously. The situation is a very entangled one. Obtaining the spectra over a wide wavelength range and at many different temperatures is certainly beneficial, but even when this is done there can remain some ambi-

guity on the assignment of levels. An analysis of the temperature dependence of the absorption cross section for individual lines can remove some ambiguities when considered in terms of Boltzmann statistics. This is best illustrated by an example. Figure 1 shows the absorption cross section dependence on temperature for two close lying lines in the $^5I_7$ manifold of Ho:YAG. The temperature dependence is different in behavior for these two lines. The line at 1847.7 nm initially shows a rise with increasing temperature, but then declines steadily after 100K. The line at 1853.6 nm always decreases with increasing temperature. The later indicates a level that terminates at the lowest Stark level of the ground manifold, the $^5I_8$, in this case. The former terminates at some level above the zero level ground state. This behavior of the absorption cross section is the same as the fractional population predicted by Boltzmann statistics and is very useful for assigning levels that have some ambiguity, and especially for finding levels that terminate to the lowest lying levels of zero energy in the ground state.

To understand how this comes about, consider the equation for Boltzmann statistics. The thermal population or Boltzmann fraction inside a manifold is given by

$$f_i = \frac{exp(E_i/kT)}{\sum_j exp(E_j/kT)} \tag{1}$$

where f_i is the fraction thermally excited in the ith Stark level within a given manifold. E_i is the energy in cm^{-1} of the ith Stark level within a given manifold. k is Boltzmann's constant and T is the temperature. The summation over j, known as the partition function, sums over all thermally populated Stark levels in the manifold. For a transition that terminates on the lowest level in the ground manifold, there will always be a decrease in thermal population, and hence cross section, with increasing temperature, since excitations have no where to go but to higher lying Stark levels. For a transition that does not terminate on the lowest level of the ground state, there will be an initial rise in population as the temperature is raised, followed by a decline as excitations move to even higher Stark levels.

While such considerations of the temperature dependent absorption spectra can reveal how to assign the levels of a great many excited Stark transitions, the emission spectra are also very valuable, especially in determining the positions of the Stark levels of the ground state. By comparing spectra in emission with those of absorption, the positions of the ground state Stark levels can be deduced for the most part. In most practical situations there will remain some ambiguity in assigning an energy to all levels, but usually those lying highest and lowest can be ascertained. It is common to find some in the middle of he ground manifold remaining undetermined experimentally. In the case of YAG,

the Stark effect is quite strong and the majority of transition lines can be resolved at very low temperatures. Nevertheless, there remain some levels which could not be determined either because they overlap with other transitions or are too weak to be seen. Thus, there remain some undefined experimental levels in the tables that are presented later in this article.

The experimental energy levels of Ho:YAG and Ho:LuAG were measured from emission and absorption spectra at temperatures ranging from 10K to 300K. As a representative example, the temperature dependence of the absorption spectra of the Ho $^5I_7$ manifold are shown in figures 2 and 3. Figure 2 shows the absorption cross section from 10 to 100K. Figure 3 shows absorption cross section from 125 to 300K. It is clear from the figures that many of the spectral lines at the lower wavelength range decrease in absorption cross section with increasing temperature, while those in the upper wavelength range increase with increasing temperature. This is consistent with the Boltzmann statistics that governs the distribution of thermal population among the Stark levels inside a manifold. To illustrate the complexity of the spectra even at very low temperatures approaching 8-10K, figure 4 shows the absorption cross section for the 6 lowest manifolds in Ho:LuAG, excluding the Ho $^5I_4$ manifold, which exhibits no absorption. It should be mentioned that the observed spectra did not show any hypersensitive transitions in changing the host material from YAG to LuAG, nor was there any clear evidence of multiple sites, although some spectra did show weak transitions that could be interpreted as due to minority sites with a symmetry other than D_2, but these instances were not commonly observed in the spectra.

In the process of measuring the energy levels of Ho:LuAG, the levels of Ho:YAG have also been measured. While there are no previous studies to compare the Ho:LuAG measurements to, a discrepancy has been found between the Ho:YAG levels measured here and those published by Gruber et al. It is difficult to understand this discrepancy. Gruber and colleagues did a thorough job in two articles and reported on the energy levels of the 50 lowest Stark split manifolds. It is somewhat disconcerting, however, that the agreement between experimental and calculated levels in Gruber's second article published in 1995[12] is worse than in his first article published in 1991[11]. The fit in the second article, for example, is particularly bad for the $^5I_7$ manifold, with differences in the measured and calculated levels ranging consistently between 15 to 25 cm^{-1}. On comparison with Gruber's first publication on the energy levels of Ho:YAG, the results presented here are in reasonable agreement, but with occasional discrepancy. The discrepancy does not seem to be in the energy of the various transitions, but in their placement within the various manifolds in some instances. The analysis presented here is considered to be very thorough as well, and the discrepancy can only be explained by a different interpretation of the spectra. In a sense, this is understandable in the context of interpreting a large number of spectral lines and assigning them an energy value based on

trends in the temperature and concentration dependent spectra. The results presented here for Ho:YAG, as a consequence, offer new placements of some of the energy levels. Some confidence in the results presented here can be gained, however, in the fact that both Ho:LuAG and Ho:YAG have been examined and show consistent placements of the levels. Future studies will have to determine the accuracy of Gruber's results versus the results presented here. The confidence in the results presented here rest on the observations of Ho in two crystal hosts, LuAG and YAG, each exhibiting similar positions of the levels.

4 Crystal Field Analysis

In order to determine values for energy levels that cannot be determined experimentally, and to check for accuracy of the assignment of experimental energy levels, a crystal field analysis is necessary. This analysis can aid in solving ambiguities in initial assignments and is an iterative process, refining the location of the energy levels and approaching an accurate assessment of the level placements. Some theoretical basis for this procedure is covered here for completeness in understanding the process. An iterative least squares fitting procedure between the experimental levels that can be measured, and those generated from a suitable set of crystal field parameters can be performed using crystal field theory. It is sometimes necessary to re-examine the spectral data if the fitting is bad for particular levels. The crystal field Hamiltonian can be written as

$$H_{CF} = \sum_{k,m} B_{km}^{\dagger} \sum_{i} C_{km}(i) \tag{2}$$

where B_{km} are the crystal-field parameters satisfying

$$B_{km}^{\dagger} = (-1)^m B_{k,-m} \tag{3}$$

and C_{km} are spherical tensors defined in terms of spherical harmonics, $Y_{km}(\theta_i, \phi_i)$, according to

$$C_{km}(i) = \left(\frac{4\pi}{2k+1}\right)^{1/2} Y_{km}(\theta_i, \phi_i) \tag{4}$$

In (2) the sums on k and m run over k=2,4,6 and m=0,$\pm$2,...,$\pm$k, and the sum on i runs over the number of electrons in the $4f^n$ configuration. In (4),

θ_i and ϕ_i are the angular coordinates of the ith electron. The B_{km} used for the determination of energy levels are always even in k because the even parts of the expansion of the crystal field potential contribute to the splitting and shifting of energy levels, while the odd parts are responsible for the mixing of opposite parity states from higher lying configurations into the $4f^n$ configuration. The later odd order terms are important for the Judd-Ofelt theory, which is discussed in the next section. It is noted that k=0 is always ignored because it represents a spherically symmetric crystal field that shifts all energy levels equally without affecting the energy level splitting. It is the crystal-field parameters, B_{km}, that describes the effects of the crystal field on the free ion Hamiltonian. The free ion Hamiltonian used in this analysis has the form

$$H_{FI} = \sum_{k=0}^{3} e_k E^k + \alpha L(L+1) + \beta G(G_2) + \gamma G(G_7) + \zeta \sum_{i=1}^{N} (\vec{s}_i \cdot \vec{l}_i) \qquad (5)$$

The first term in (5) represents the electron-electron intra-shell Coulomb interaction between 4f electrons. The second, third and fourth terms are 2-body electron-electron configuration interaction terms representing interactions between electron configurations of the same parity. The fifth term is the spin-orbit coupling, representing the magnetic dipole-dipole interactions between the spin and angular magnetic moments of the 4f electrons. This is a seven parameter free-ion Hamiltonian. E^k (k=1,2,3) are the Racah parameters corresponding to linear combinations of Slater radial integrals. α, β, and γ are parameters corresponding to linear combinations of radial factors and excitation energies of the 4f-electrons to the electrons of the perturbing configuration. These parameters are sometimes referred to as 'Trees' parameters. ζ is the spin-orbit parameter, which is a radial integral. All of these parameters contain the radial dependence of the Hamiltonian. The angular dependence of the Hamiltonian is expressed in the operators e_k, L^2, $G(G_2)$, $G(R_7)$, and $\vec{s} \cdot \vec{l}$. These are, respectively, the angular spherical harmonic operators of the Coulomb potential, the angular momentum operator, the Casimir operator for Lie group G_2, the Casimir operator for Lie group R_7, and the spin-orbit operator. This separation of the free-ion Hamiltonian into radial parameters and angular operators is done because reliable radial wavefunctions can not be generated. Instead, the radial parts of the Hamiltonian are treated as adjustable parameters. Even if reliable electrostatic and spin-orbit radial wavefunctions were known, the configuration interaction would still present a problem.

The analysis done here has used software originally developed at the Harry Diamond Laboratory (HDL), now the Army Research Laboratory (ARL), in Adelphi, MD. This software was originally developed in the 1970's by Clyde Morrison, Richard Leavitt and Nick Karayanis, and has been utilized and further developed at NASA Langley Research Center since the 1980's. Repre-

sentative articles covering applications using this software can be found in two articles by Morrison and Leavitt[13,14]. Free-ion wavefunctions in a Russel-Saunders basis were calculated by diagonalizing the Hamiltonian given in (5). The free-ion parameters used were those given by Carnall, Fields and Rajnak for Ho in aqueous solution[15]. The Russel-Saunders (SLJ) wavefunctions were used as basis states to form a linear superposition of states for intermediate coupling ([SL]J), from which the reduced matrix elements of $U^{(2)}$, $U^{(4)}$, $U^{(6)}$ between all the intermediate-coupled wavefunctions for the $4f^{12}$ free-ion configuration of Ho were calculated. Nine manifolds were used in a truncated set of intermediate-coupled states to set up the crystal space for the D_2 crystal-field symmetry appropriate for YAG, and LuAG. The crystal field Hamiltonian given in (2) is diagonalized together with an effective free-ion Hamiltonian of the form

$$H_{FI} = \sum_{[SL]J} E_{[SL]J} |\, [SL]J\rangle\langle [SL]J \,| \tag{6}$$

where $E_{[SL]J}$ are the centroids of the energy manifolds. The free-ion values of the centroids are used as initial parameters.

The fitting procedure of experimental and theoretical energy levels consists of first fitting the centroids while keeping the crystal field parameters constant. This adjusts the free-ion centroid positions of the manifolds to their approximate value for the ion in the presence of the crystal field of the host. The fit then proceeds by letting the crystal field parameters vary in an iterative process until a least squares minimum is obtained between the calculated and measured energy levels. The initial value of the crystal field parameters can be approximated theoretically[13], but we used the crystal field parameters of Gruber et al.[11] for Ho:YAG as an initial guess in the energy level fitting.

The crystal field parameters were varied to determine the best fit between experimental and theoretical energy levels. The crystal field parameters determined from the energy level fitting in Ho:YAG and Ho:LuAG are given in table 2. The crystal field parameters for Ho:YAG determined by Gruber et al.[11] are also given in this table for comparison. Due to the difference between the results of Gruber and those presented here, some difference is expected, but the parameters are in fair agreement. The experimental and theoretical energy levels for the first 9 manifolds, the $^5I_8$ ground state through the $^5F_4$ excited state, for Ho:YAG and Ho:LuAG are given in tables 3 and 4, respectively. The second column in these tables is the irreducible representation (I.R.) of the Stark level. Note that there are no degeneracies in the energy level structure. The I.R. can be used to determine the selection rules for Stark level to Stark level transitions. The selection rules for electric dipole-dipole transitions in D_2 symmetry are shown in table 1. The energy level diagram

for the Ho $^5I_7$ excited manifold and the Ho $^5I_8$ ground manifold of Ho:YAG and Ho:LuAG is shown in figure 5 for comparison.

5 Judd Ofelt Analysis

The theory of Judd and Ofelt[16,17] has been applied to the optical absorption intensities in Ho:YAG and Ho:LuAG. The utility of the Judd-Ofelt theory is that it provides a theoretical expression for the line strength, given by

$$S_{ED}(aJ;bJ') = \sum_{\lambda=2,4,6} \Omega_\lambda | \langle f^n[SL]J \mid\mid U^{(\lambda)} \mid\mid f^n[S'L']J' \rangle |^2 \tag{7}$$

where Ω_λ are the Judd-Ofelt parameters. The term in brackets are doubly reduced matrix elements for intermediate coupling. Intermediate coupling refers to a situation where the mutual repulsion interaction between 4f electrons is of the same order of magnitude as the spin-orbit coupling. This effect can be incorporated by expanding the wavefunctions of the 4f states in a linear combination of Russel Saunders, or LS coupled states. The coupling coefficients are found by diagonalizing the combined electrostatic, spin orbit and configuration interaction energy matrices to obtain the full intermediate coupled wavefunctions, $\mid f^n[SL]\rangle$. A substantial portion of the book 'Spectroscopic coefficients of the p^n, d^n, and f^n configurations' by Nielson and Koster[18] is devoted to tabulating matrix elements in LS coupling. Further efforts must be devoted to converting these wavefunctions to the intermediate coupling case applicable to lanthanide ions. Fortunately, many references tabulate intermediate coupled matrix elements based on Nielson and Koster's work. Because the electric dipole transitions arise from a small crystal field perturbation, the matrix elements are not highly dependent on the host material. The experimental linestrength is found from

$$S_m = \frac{3hc(2J'+1)}{8\pi^3 e^2 \bar{\lambda}} n \left(\frac{3}{n^2+2}\right)^2 \int \sigma(\lambda) d\lambda \tag{8}$$

where J' is the total angular momentum of the initial ground manifold, found from the $^{2S+1}L_J$ designation. $\sigma(\lambda)$ is the emission cross section as a function of wavelength. The mean wavelength, $\bar{\lambda}$, can be found from the first moment of the absorption cross section data

$$\bar{\lambda} = \frac{\sum \sigma(\lambda)}{\sum \lambda \sigma(\lambda)} \tag{9}$$

The other symbols have their usual meaning.

The Judd-Ofelt parameters, Ω_λ form a set of phenomenological parameters to be determined from fitting experimental absorption measurements determined in (8) with the theoretical Judd-Ofelt expression in (7). The least squares fitting procedure has been carried out for Ho:YAG and Ho:LuAG. The results of the fit are shown in tables 5 and 7, respectively. The transition probabilities follow from

$$A(aJ;bJ') = \frac{64\pi^4 e^2}{3h(2J+1)\bar{\lambda}^3}\left[n\left(\frac{n^2+2}{3}\right)^2 S_{ED}(aJ;bJ') + n^3 S_{MD}(aJ;bJ')\right] \quad (10)$$

where n is the index of refraction of the solid, and $S_{ED}(aJ;bJ')$ and $S_{MD}(aJ;bJ')$ represent the electric and magnetic dipole line strengths. In this equation J represents the total angular momentum of the upper excited state. Electric dipole linestrengths, S_{ED} were calculated from each excited manifold to all lower lying manifolds using (7) along with the relevant matrix elements and the Judd-Ofelt parameters extracted from the fit. Magnetic dipole linestrengths were calculated in a straightforward way from angular momentum considerations.[19] These values were then converted to intermediate coupling values using the free ion wavefunctions for triply ionized holmium.[20] The calculation of magnetic dipole linestrengths, S_{MD}, in intermediate coupling has been covered in a previous article by one of the authors.[21] The radiative lifetimes, τ_r, follow from

$$\tau_r = \frac{1}{\sum_{J'} A(J,J')} \quad (11)$$

and the branching ratios, β, follow from

$$\beta_{JJ'} = \frac{A(J,J')}{\sum_{J'} A(J,J')} \quad (12)$$

The results of these calculations for the first nine manifolds in Ho:YAG and Ho:LuAG are shown in tables 6 and 8, respectively. In addition, some measured lifetimes at low temperature, 20K, appear in the last column. Even at very low temperatures, nonradiative quenching of the lifetime occurs, so agreement between the Judd-Ofelt and measured lifetimes are not always expected to be in agreement. This is especially true the smaller is the energy gap to the next lower lying manifold. The gap between the $^5I_7$ and $^5I_8$ is the largest by far. In this case the Judd-Ofelt values and the low temperature lifetime for

the $^5I_7$ manifold are in good agreement. Overall, the results are quite good, and within the range of error associated with the Judd-Ofelt theory. Finally, the Judd-Ofelt parameters for this analysis are tabulated along with other sets from the literature for Ho:YAG and Ho:LuAG, and are shown in table 9. The Judd-Ofelt parameters measured here for Ho:YAG and Ho:YLF are in reasonable agreement with previous studies[22,23]. As might be expected the Judd-Ofelt parameters are indeed very similar for Ho:YAG and its isomorph Ho:LuAG.

6 Summary

The energy levels of Ho^{3+} ions in Ho:YAG and Ho:LuAG have been measured, the later has not been measured previously. Crystal field parameters were varied to determine the best fit between experimental and theoretical energy levels. The energy levels of the first 9 manifolds of Ho:YAG and Ho:LuAG have been determined here as well as the crystal field parameters for Ho:YAG and Ho:LuAG. While there are no previous measurements to compare our measurements of Ho:LuAG with, some discrepancies with earlier studies of Ho:YAG have been discussed here. Self-consistency between the Ho:YAG and Ho"LuAG energy levels measured here serve as an indication that the earlier studies may have some incorrect assignments. This article provides useful information to those doing research involving trivalent Ho ions in the garnet isomorphs YAG and LuAG. A knowledge of the energy levels is an indispensable piece of information when considering a laser ion in a given host material. The energy levels of Ho:LuAG are seen to be very similar to those in Ho:YAG. However, subtle changes resulting from replacing Y with Lu in the garnet crystal Ho:YAG results in slightly different transition wavelengths than in Ho:LuAG. The energy levels for Ho:LuAG measured here indicate that Ho:LuAG lasers will have a slightly reduced lower laser thermal population than Ho:YAG for improved performance of $^5I_7 \rightarrow {}^5I_8$ lasing at $\sim 2.1\ \mu$m compared to Ho:YAG. In general, the energy levels and intensity parameters measured here should be of interest to those in the spectroscopy and laser community doing research with Ho^{3+} ions in $Y_3Al_5O_{12}$ and $Lu_3Al_5O_{12}$.

7 References

References

[1] M.E. Storm, Laser Focus World 27(4)(1991) 117.

[2] N.P. Barnes, Laser Focus World 31(4)(1991) 87.

[3] B. Struve, G. Huber, J. Phys. IV 1 (1991) 3

[4] K. Azawu, Rev. Laser Eng. 26 (2000) 291.

[5] M.G. Jani, N.P. Barnes, K.E. Murray, R.L. Hutcheson, ASSL Trends in Optics and Photonics 20 (1994) 109.

[6] M.G. Jani, N.P. Barnes, K.E. Murray, D.W. Hart, G.J. Quarles, V.K. Castillo, IEEE J. Quant. Elec. 33 (1997) 112.

[7] N.P. Barnes, E.D. Filer, F.L. Naranjo, W.J. Rodriguez, M.R. Kokta, Opt. Lett. 18 (1993) 708.

[8] E.D. Filer, C.A. Morrison, N.P. Barnes, B.M. Walsh, ASSL Trends in Optics and Photonics 20 (1994) 127.

[9] R.D. Shannon, Acta Cryst. 32 (1976) 751.

[10] Y. Kuwano, K. Suda, N. Ishizawa, T. Yamada, J. Cryst. Growth 260 (2003) 159.

[11] J.B. Gruber, M.E. Hills, M.D. Seltzer, S.B. Stevens, C.A. Morrison, G.A. Turner, M.R. Kokta, J. Appl. Phys. 69 (1991) 8183.

[12] J.B. Gruber, M.D. Seltzer, V.J. Pugh, F.S. Richardson, J. Appl. Phys. 77 (1995) 5882.

[13] C.A. Morrison, R.P. Leavitt J. Chem. Phys. 71 (1979) 2366.

[14] R.P. Leavitt, C.A. Morrison J. Chem. Phys. 73 (1980) 749.

[15] W.T. Carnall, P.R. Fields, K. Rajnak, J. Chem. Phys. 49 (1968) 4424.

[16] B.R. Judd, Phys. Rev. 127 (1962) 750.

[17] G.S. Ofelt, J. Chem. Phys. 37 (1962) 511.

[18] C.W. Nielson, G.F. Koster, The M.I.T. Press, Cambridge, MA (1963)

[19] G.H. Shortly, Phys. Rev. 57 (1940) 225.

[20] K. Rajnak, W.J. Krupke J. Chem. Phys. 46 (1967) 3532.

[21] B.M. Walsh, N.P. Barnes, B. Di Bartolo, J. Appl. Phys. 83 (1998) 2772.

[22] M. Malinowski, Z. Frukacz, M. Szuflinska, A. Wnuk, M. Kaczkan, J. Alloys and Compounds 300-301 (2000) 389.

[23] D.N. Patel, B.R. Brody, S.K. Nash-Stevenson, Opt. Mat. 10 (1998) 225.

Table 1
Selection rules for electric dipole transitions in D_2 symmetry.

	Γ_1	Γ_2	Γ_3	Γ_4
Γ_1	forbidden	$\surd$	$\surd$	$\surd$
Γ_2	$\surd$	forbidden	$\surd$	$\surd$
Γ_3	$\surd$	$\surd$	forbidden	$\surd$
Γ_4	$\surd$	$\surd$	$\surd$	forbidden

Table 2
Crystal field parameters in Ho:YAG and Ho:LuAG.

Material	B_{20}	B_{22}	B_{40}	B_{42}	B_{44}	B_{60}	B_{62}	B_{64}	B_{66}
Ho:YAG[11]	554	73	-228	-1543	-811	-1028	-382	609	-343
Ho:YAG	592	28	-62	-1342	-696	-1158	-430	547	-405
Ho:LuAG	469	8	-51	-1360	-711	-1177	-445	573	-449

Table 3: Experimental and theoretical energy levels in Ho:YAG at 8K.

level	I.R.	Energy (theo.) (cm^{-1})	Energy (exp.) (cm^{-1})	Centroid (cm^{-1})	Free Ion mixture
1	Γ_2	1.0	0.0		99.89 5I8 + 0.07 5I7 + 0.01 5F5
2	Γ_2	4.4	3.8		99.89 5I8 + 0.08 5I7 + 0.01 5F5
3	Γ_1	46.9	41.8		99.94 5I8 + 0.02 5I7 + 0.01 5F5
4	Γ_3	56.5	52.9		99.93 5I8 + 0.03 5I7 + 0.02 5F5
5	Γ_2	141.4	143.8		99.92 5I8 + 0.03 5I7 + 0.01 5G6
6	Γ_1	160.8	152.6		99.93 5I8 + 0.02 5F5 + 0.01 5G6
7	Γ_3	162.3	160.8		99.90 5I8 + 0.04 5I7 + 0.02 5F5
8	Γ_4	167.6	162.8	5I8	99.90 5I8 + 0.03 5F5 + 0.03 5I7
9	Γ_2	414.8	415.0	(315)	99.57 5I8 + 0.39 5I7 + 0.01 5G6
10	Γ_4	435.5	443.0		99.65 5I8 + 0.28 5I7 + 0.04 5I6
11	Γ_1	456.8	456.0		99.69 5I8 + 0.25 5I7 + 0.03 5I6
12	Γ_3	458.8	462.0		99.73 5I8 + 0.18 5I7 + 0.07 5I6
13	Γ_1	495.8	498.0		99.76 5I8 + 0.13 5I7 + 0.07 5I6
14	Γ_2	497.9	507.0		99.72 5I8 + 0.20 5I7 + 0.06 5I6
15	Γ_1	522.1	520.0		99.68 5I8 + 0.26 5I7 + 0.03 5I6
16	Γ_3	534.7	537.0		99.65 5I8 + 0.30 5I7 + 0.03 5F4
17	Γ_4	540.5	542.0		99.71 5I8 + 0.23 5I7 + 0.03 5F4
18	Γ_4	5230.5	5228.0		99.53 5I7 + 0.33 5I8 + 0.07 5F5
19	Γ_2	5232.1	5230.0		99.56 5I7 + 0.33 5I8 + 0.07 5F5
20	Γ_3	5245.0	5243.0		99.55 5I7 + 0.30 5I8 + 0.06 5I6
21	Γ_1	5252.1	5251.0		99.51 5I7 + 0.39 5I8 + 0.06 5I6
22	Γ_3	5303.3	5302.0		99.62 5I7 + 0.16 5I8 + 0.12 5I6
23	Γ_4	5312.0	5311.0		99.53 5I7 + 0.22 5I6 + 0.17 5I8
24	Γ_2	5320.0	5320.0	5I7	99.59 5I7 + 0.26 5I8 + 0.06 5I6

continued on next page

Table 3: *continued*

level	I.R.	Energy (theo.) (cm^{-1})	Energy (exp.) (cm^{-1})	Centroid (cm^{-1})	Free Ion mixture
25	Γ_1	5339.6	5340.0	(5346)	99.65 5I7 + 0.27 5I8 + 0.02 5I6
26	Γ_2	5350.0	5351.0		99.41 5I7 + 0.46 5I6 + 0.05 5I8
27	Γ_1	5373.2	5373.0		99.31 5I7 + 0.59 5I6 + 0.03 5I5
28	Γ_4	5375.1	5375.0		99.39 5I7 + 0.38 5I6 + 0.12 5I5
29	Γ_3	5393.4	5396.0		99.38 5I7 + 0.43 5I6 + 0.09 5I5
30	Γ_2	5404.3	5408.0		99.48 5I7 + 0.24 5I6 + 0.19 5I5
31	Γ_3	5453.1	5454.0		99.45 5I7 + 0.35 5I6 + 0.11 5I5
32	Γ_4	5454.8	5456.0		99.46 5I7 + 0.31 5I6 + 0.16 5I5
33	Γ_1	8740.2	8741.0		99.35 5I6 + 0.30 5I7 + 0.17 5I5
34	Γ_3	8744.1	8745.0		99.20 5I6 + 0.37 5I5 + 0.31 5I7
35	Γ_4	8764.6	8766.0		99.16 5I6 + 0.41 5I5 + 0.32 5I7
36	Γ_1	8770.1	-		99.21 5I6 + 0.55 5I5 + 0.08 5I4
37	Γ_3	8772.3	8775.0		98.97 5I6 + 0.54 5I5 + 0.34 5I7
38	Γ_2	8772.4	8774.0	5I6	99.22 5I6 + 0.34 5I7 + 0.26 5I5
39	Γ_4	8817.4	8821.0	(8837)	99.34 5I6 + 0.27 5I7 + 0.19 5I5
40	Γ_1	8842.5	8843.0		98.96 5I6 + 0.61 5I5 + 0.23 5I4
41	Γ_2	8859.4	8859.0		98.85 5I6 + 0.76 5I5 + 0.21 5I4
42	Γ_4	8875.9	8872.0		99.17 5I6 + 0.32 5I7 + 0.28 5I5
43	Γ_3	8879.1	8879.0		99.21 5I6 + 0.31 5I7 + 0.22 5I4
44	Γ_1	8944.9	8943.0		99.27 5I6 + 0.25 5I5 + 0.24 5I7
45	Γ_2	8962.3	8957.0		99.50 5I6 + 0.31 5I7 + 0.10 5I5
46	Γ_4	11309.4	11313.0		99.36 5I5 + 0.27 5I6 + 0.21 5I7
47	Γ_2	11315.2	11318.0		98.75 5I5 + 0.64 5I6 + 0.36 5I4
48	Γ_2	11339.1	-		98.38 5I5 + 1.27 5I4 + 0.18 5I6
49	Γ_3	11343.5	11341.0		99.41 5I5 + 0.18 5I6 + 0.17 5I7

continued on next page

Table 3: *continued*

level	I.R.	Energy (theo.) (cm^{-1})	Energy (exp.) (cm^{-1})	Centroid (cm^{-1})	Free Ion mixture
50	Γ_4	11347.2	11348.0	5I5	97.11 5I5 + 2.70 5I4 + 0.08 5I7
51	Γ_1	11348.5	11351.0	(11389)	98.66 5I5 + 0.83 5I6 + 0.33 5I4
52	Γ_2	11383.4	11387.0		98.59 5I5 + 0.90 5I4 + 0.27 5I6
53	Γ_3	11390.9	11390.0		97.96 5I5 + 1.74 5I4 + 0.17 5I6
54	Γ_1	11430.0	11425.0		98.53 5I5 + 0.67 5I6 + 0.65 5I4
55	Γ_4	11478.0	11478.0		98.55 5I5 + 0.71 5I4 + 0.56 5I6
56	Γ_3	11478.9	11473.0		98.67 5I5 + 0.66 5I6 + 0.49 5I4
57	Γ_2	13265.2	13266.0		99.02 5I4 + 0.54 5I5 + 0.28 5I6
58	Γ_1	13322.3	13325.0		98.96 5I4 + 0.56 5I5 + 0.31 5I6
59	Γ_3	13343.8	13348.0		99.02 5I4 + 0.46 5I5 + 0.25 5I6
60	Γ_1	13367.0	13367.0	5I4	99.12 5I4 + 0.32 5I5 + 0.19 5I6
61	Γ_4	13387.1	13389.0	(13441)	98.35 5I4 + 1.20 5I5 + 0.18 5I6
62	Γ_4	13500.6	-		97.60 5I4 + 2.21 5I5 + 0.05 5F3
63	Γ_3	13560.9	13554.0		98.09 5I4 + 1.82 5I5 + 0.03 5F1
64	Γ_2	13586.0	-		97.94 5I4 + 1.96 5I5 + 0.03 5F3
65	Γ_1	13788.8	13786.0		99.82 5I4 + 0.07 5F4 + 0.06 5I6
66	Γ_3	15454.2	15457.0		99.64 5F5 + 0.14 5F3 + 0.08 5F4
67	Γ_2	15455.8	15458.0		99.64 5F5 + 0.09 5F3 + 0.06 5F4
68	Γ_1	15471.0	15473.0		99.49 5F5 + 0.15 5F4 + 0.08 5F2
69	Γ_4	15482.2	15488.0		99.56 5F5 + 0.21 5F4 + 0.08 5F3
70	Γ_2	15507.1	15516.0	5F5	99.38 5F5 + 0.32 5F4 + 0.09 5F2
71	Γ_3	15661.9	15652.0	(15598)	99.46 5F5 + 0.24 5G6 + 0.09 5I5
72	Γ_1	15669.8	15667.0		99.56 5F5 + 0.12 5G6 + 0.09 5F4
73	Γ_4	15677.4	15675.0		99.56 5F5 + 0.17 5G6 + 0.09 5I6
74	Γ_3	15699.5	15694.0		99.66 5F5 + 0.08 5I7 + 0.08 5F4

continued on next page

Table 3: *continued*

level	I.R.	Energy (theo.) (cm^{-1})	Energy (exp.) (cm^{-1})	Centroid (cm^{-1})	Free Ion mixture
75	Γ_4	15735.1	15736.0		99.77 5F5 + 0.07 5I6 + 0.06 5I7
76	Γ_2	15742.2	15740.0		99.80 5F5 + 0.07 5I7 + 0.06 5I6
77	Γ_1	18464.5	18450.0		62.11 5S2 + 37.22 5F4 + 0.28 5F2
78	Γ_2	18471.3	18459.0	5S2	67.81 5S2 + 31.43 5F4 + 0.25 5F5
79	Γ_1	18532.8	18532.0	(18531)	93.52 5S2 + 5.91 5F4 + 0.29 5G6
80	Γ_3	18535.3	18541.0		98.91 5S2 + 0.53 5F4 + 0.32 5G6
81	Γ_4	18540.0	18546.0		98.97 5S2 + 0.40 5F4 + 0.36 5G6
82	Γ_1	18570.5	18583.0		56.68 5F4 + 42.25 5S2 + 0.54 5G6
83	Γ_2	18584.2	18587.0		77.50 5F4 + 21.41 5S2 + 0.39 5F3
84	Γ_2	18614.1	18626.0		88.51 5F4 + 10.29 5S2 + 0.51 5G6
85	Γ_4	18617.7	-	5F4	98.39 5F4 + 0.73 5F3 + 0.32 5S2
86	Γ_3	18663.3	18665.0	(18655)	98.60 5F4 + 0.54 5S2 + 0.23 5F3
87	Γ_4	18700.1	18700.0		99.45 5F4 + 0.28 5G6 + 0.07 5S2
88	Γ_1	18720.4	18715.0		99.00 5F4 + 0.52 5S2 + 0.25 5G6
89	Γ_3	18735.2	18730.0		99.41 5F4 + 0.34 5G6 + 0.08 5F3
90	Γ_1	18747.0	18745.0		99.08 5F4 + 0.49 5S2 + 0.15 5G6
91	Γ_4	20593.3	20591.0		98.54 5F3 + 0.68 5F4 + 0.30 3G5
92	Γ_2	20620.0	20621.0		97.88 5F3 + 0.66 5F1 + 0.56 5F4
93	Γ_3	20634.6	20631.0	5F3	98.44 5F3 + 0.36 5F4 + 0.31 5F1
94	Γ_3	20744.2	20747.0	(20711)	96.87 5F3 + 0.61 5G6 + 0.29 5F2
95	Γ_2	20764.6	20760.0		96.24 5F3 + 3.12 5G6 + 0.45 5F2
96	Γ_4	20769.2	20777.0		98.23 5F3 + 1.33 5G6 + 0.13 5F4
97	Γ_1	20784.1	20784.0		97.36 5F3 + 1.45 5F2 + 0.86 5G6

Table 4: Experimental and theoretical energy levels in Ho:LuAG at 8K.

level	I.R.	Energy (theo.) (cm^{-1})	Energy (exp.) (cm^{-1})	Centroid (cm^{-1})	Free Ion mixture
1	Γ_2	0.9	0.0		99.88 5I8 + 0.08 5I7 + 0.01 5F5
2	Γ_2	5.0	4.5		99.88 5I8 + 0.09 5I7 + 0.01 5F5
3	Γ_1	41.8	37.9		99.93 5I8 + 0.02 5I7 + 0.01 5F5
4	Γ_3	55.4	50.8		99.92 5I8 + 0.03 5I7 + 0.02 5F5
5	Γ_2	123.0	125.7		99.91 5I8 + 0.04 5I7 + 0.01 5F5
6	Γ_3	146.0	138.6		99.90 5I8 + 0.04 5I7 + 0.02 5F5
7	Γ_1	149.5	147.7		99.93 5I8 + 0.02 5F5 + 0.01 5G6
8	Γ_4	153.5	150.8	5I8	99.90 5I8 + 0.03 5F5 + 0.03 5I7
9	Γ_2	418.8	421.3	(315)	99.55 5I8 + 0.42 5I7 + 0.01 5G6
10	Γ_4	441.6	450.0		99.64 5I8 + 0.29 5I7 + 0.04 5I6
11	Γ_1	464.2	465.0		99.64 5I8 + 0.32 5I7 + 0.01 5I6
12	Γ_3	469.2	469.0		99.72 5I8 + 0.18 5I7 + 0.07 5I6
13	Γ_2	487.3	493.6		99.70 5I8 + 0.21 5I7 + 0.06 5I6
14	Γ_1	492.1	500.0		99.81 5I8 + 0.12 5I6 + 0.05 5I7
15	Γ_1	529.2	529.2		99.63 5I8 + 0.32 5I7 + 0.03 5F4
16	Γ_3	542.0	542.0		99.63 5I8 + 0.33 5I7 + 0.03 5F4
17	Γ_4	545.6	546.0		99.69 5I8 + 0.25 5I7 + 0.03 5F4
18	Γ_4	5234.2	5231.0		99.51 5I7 + 0.33 5I8 + 0.08 5F5
19	Γ_2	5236.4	5233.0		99.55 5I7 + 0.33 5I8 + 0.07 5F5
20	Γ_3	5246.3	5244.0		99.54 5I7 + 0.30 5I8 + 0.07 5I6
21	Γ_1	5256.0	5254.0		99.48 5I7 + 0.41 5I8 + 0.06 5I6
22	Γ_3	5299.4	5298.0		99.59 5I7 + 0.20 5I8 + 0.12 5I6
23	Γ_4	5310.5	5309.0		99.54 5I7 + 0.21 5I8 + 0.17 5I6
24	Γ_2	5315.3	5316.0	5I7	99.55 5I7 + 0.33 5I8 + 0.04 5I6

continued on next page

Table 4: *continued*

level	I.R.	Energy (theo.) (cm^{-1})	Energy (exp.) (cm^{-1})	Centroid (cm^{-1})	Free Ion mixture
25	Γ_1	5332.6	5332.0	(5346)	99.62 5I7 + 0.29 5I8 + 0.02 5I6
26	Γ_2	5352.1	5352.0		99.42 5I7 + 0.48 5I6 + 0.03 5G6
27	Γ_1	5373.8	5375.0		99.28 5I7 + 0.62 5I6 + 0.03 5I5
28	Γ_4	5379.9	5381.0		99.33 5I7 + 0.45 5I6 + 0.12 5I5
29	Γ_3	5394.1	5398.0		99.33 5I7 + 0.47 5I6 + 0.10 5I5
30	Γ_2	5405.8	5411.0		99.40 5I7 + 0.28 5I6 + 0.22 5I5
31	Γ_3	5442.2	5443.0		99.41 5I7 + 0.38 5I6 + 0.12 5I5
32	Γ_4	5444.4	5446.0		99.41 5I7 + 0.33 5I6 + 0.18 5I5
33	Γ_1	8746.2	8746.0		99.37 5I6 + 0.29 5I7 + 0.13 5I5
34	Γ_3	8751.3	8751.0		99.11 5I6 + 0.50 5I5 + 0.27 5I7
35	Γ_4	8759.0	8760.0		99.14 5I6 + 0.43 5I5 + 0.31 5I7
36	Γ_1	8765.9	-		99.16 5I6 + 0.58 5I5 + 0.07 5I4
37	Γ_3	8767.0	8769.0		99.03 5I6 + 0.41 5I7 + 0.38 5I5
38	Γ_2	8770.1	8769.0	5I6	99.18 5I6 + 0.35 5I7 + 0.27 5I5
39	Γ_4	8810.7	8813.0	(8835)	99.32 5I6 + 0.30 5I7 + 0.18 5I5
40	Γ_1	8839.4	8843.0		98.84 5I6 + 0.71 5I5 + 0.26 5I4
41	Γ_2	8856.1	8857.0		98.72 5I6 + 0.86 5I5 + 0.24 5I4
42	Γ_4	8877.5	8876.0		99.09 5I6 + 0.35 5I7 + 0.32 5I5
43	Γ_3	8879.2	8880.0		99.13 5I6 + 0.33 5I7 + 0.23 5I4
44	Γ_1	8934.2	8931.0		99.22 5I6 + 0.27 5I7 + 0.25 5I5
45	Γ_2	8957.2	8953.0		99.51 5I6 + 0.35 5I7 + 0.07 5I5
46	Γ_4	11315.4	11318.0		99.36 5I5 + 0.25 5I6 + 0.24 5I7
47	Γ_2	11322.1	11324.0		98.83 5I5 + 0.70 5I6 + 0.17 5I7
48	Γ_2	11335.9	11334.0		98.30 5I5 + 1.38 5I4 + 0.18 5I6
49	Γ_3	11339.6	-		99.42 5I5 + 0.18 5I7 + 0.16 5I6

continued on next page

Table 4: *continued*

level	I.R.	Energy (theo.) (cm^{-1})	Energy (exp.) (cm^{-1})	Centroid (cm^{-1})	Free Ion mixture
50	Γ_1	11343.2	11343.0	5I5	98.63 5I5 + 0.87 5I6 + 0.31 5I4
51	Γ_4	11344.3	11345.0	(11388)	96.95 5I5 + 2.88 5I4 + 0.07 5I7
52	Γ_2	11376.3	11382.0		98.36 5I5 + 1.11 5I4 + 0.27 5I6
53	Γ_3	11383.5	11385.0		97.68 5I5 + 2.03 5I4 + 0.14 5I6
54	Γ_1	11432.6	11429.0		98.41 5I5 + 0.72 5I6 + 0.71 5I4
55	Γ_4	11470.1	11469.0		98.48 5I5 + 0.72 5I4 + 0.61 5I6
56	Γ_3	11471.7	11466.0		98.64 5I5 + 0.73 5I6 + 0.44 5I4
57	Γ_2	13256.4	13262.0		99.02 5I4 + 0.51 5I5 + 0.31 5I6
58	Γ_1	13319.4	13324.0		99.04 5I4 + 0.47 5I5 + 0.33 5I6
59	Γ_3	13347.8	13346.0		99.00 5I4 + 0.44 5I5 + 0.27 5I6
60	Γ_1	13357.2	13357.0	5I4	98.95 5I4 + 0.45 5I5 + 0.20 5I6
61	Γ_4	13383.8	13383.0	(13438)	98.40 5I4 + 1.09 5I5 + 0.20 5I6
62	Γ_4	13502.8	-		97.35 5I4 + 2.46 5I5 + 0.05 5F3
63	Γ_3	13563.2	13558.0		97.84 5I4 + 2.07 5I5 + 0.03 5F1
64	Γ_2	13574.9	-		97.79 5I4 + 2.11 5I5 + 0.03 5F3
65	Γ_1	13795.2	13793.0		99.82 5I4 + 0.08 5F4 + 0.07 5I6
66	Γ_3	15451.3	15454.0		99.64 5F5 + 0.14 5F3 + 0.08 5F4
67	Γ_2	15454.0	15456.0		99.62 5F5 + 0.10 5F3 + 0.08 5F4
68	Γ_1	15469.4	15473.0		99.49 5F5 + 0.16 5F4 + 0.08 5F2
69	Γ_4	15475.4	15480.0		99.58 5F5 + 0.18 5F4 + 0.09 5F3
70	Γ_2	15501.1	15509.0	5F5	99.41 5F5 + 0.29 5F4 + 0.09 5F2
71	Γ_3	15663.8	15659.0	(15594)	99.49 5F5 + 0.21 5G6 + 0.09 5I5
72	Γ_1	15666.0	15662.0		99.58 5F5 + 0.12 5G6 + 0.07 5I5
73	Γ_4	15684.2	15676.0		99.57 5F5 + 0.15 5G6 + 0.09 5I6
74	Γ_3	15701.7	15697.0		99.68 5F5 + 0.09 5I7 + 0.07 5I6

continued on next page

Table 4: *continued*

level	I.R.	Energy (theo.) (cm^{-1})	Energy (exp.) (cm^{-1})	Centroid (cm^{-1})	Free Ion mixture
75	Γ_4	15726.0	15727.0		99.76 5F5 + 0.07 5I6 + 0.07 5I7
76	Γ_2	15733.2	-		99.80 5F5 + 0.07 5I7 + 0.06 5I6
77	Γ_1	18460.1	18444.0		64.87 5S 2 + 34.51 5F4 + 0.22 5F2
78	Γ_2	18464.8	18450.0	5S2	67.58 5S 2 + 31.72 5F4 + 0.24 5F5
79	Γ_1	18528.2	18529.0	(18525)	94.60 5S 2 + 4.84 5F4 + 0.28 5G6
80	Γ_3	18529.9	18535.0		98.90 5S 2 + 0.53 5F4 + 0.33 5G6
81	Γ_4	18534.6	18541.0		98.88 5S 2 + 0.47 5F4 + 0.37 5G6
82	Γ_1	18568.4	18586.0		60.42 5F 4 + 38.50 5S2 + 0.60 5G6
83	Γ_2	18583.8	18588.0		72.81 5F 4 + 26.03 5S2 + 0.40 5G6
84	Γ_2	18608.3	18615.0		93.06 5F 4 + 5.89 5S2 + 0.41 5G6
85	Γ_4	18611.5	18618.0	5F4	98.31 5F 4 + 0.72 5F3 + 0.42 5S2
86	Γ_3	18653.1	18654.0	(18649)	98.56 5F 4 + 0.52 5S2 + 0.32 5F3
87	Γ_4	18701.4	18700.0		99.51 5F 4 + 0.27 5G6 + 0.05 5S2
88	Γ_1	18717.4	18713.0		99.07 5F 4 + 0.49 5S2 + 0.27 5G6
89	Γ_3	18726.8	18721.0		99.45 5F 4 + 0.36 5G6 + 0.04 5F3
90	Γ_1	18738.6	18733.0		99.21 5F 4 + 0.41 5S2 + 0.12 5G6
91	Γ_4	20586.6	20590.0		98.53 5F 3 + 0.70 5F4 + 0.28 3G5
92	Γ_2	20603.7	20609.0		98.53 5F 3 + 0.54 5F4 + 0.50 5F1
93	Γ_3	20627.7	20628.0	5F3	98.51 5F 3 + 0.40 5F4 + 0.32 5F1
94	Γ_3	20739.4	20744.0	(20698)	98.85 5F 3 + 0.70 5G6 + 0.15 5F2
95	Γ_2	20765.1	20753.0		96.40 5F 3 + 3.23 5G6 + 0.21 5F2
96	Γ_4	20768.2	20766.0		98.27 5F 3 + 1.33 5G6 + 0.10 5F4
97	Γ_1	20781.7	20782.0		97.80 5F 3 + 1.00 5F2 + 0.88 5G6

Table 5
Measured and calculated values for the Linestrength in Ho^{3+} YAG.

Transition (from $^5I_8$)	$\mid \langle U^{(2)} \rangle \mid^2$	$\mid \langle U^{(4)} \rangle \mid^2$	$\mid \langle U^{(6)} \rangle \mid^2$	$\bar{\lambda}$(nm)	Linestrength(10^{-20} cm^2)	
					measured	calculated
$^3K_6 + {}^3F_4$	0.0026	0.1263	0.0073	334	0.2600	0.2760
$^3L_9 + {}^5G_3$	0.0185	0.0052	0.1169	347	0.2411	0.3004
$^3D_2 + {}^3H_6 + {}^5G_5$	0.2155	0.1969	0.1679	362	0.8480	0.7218
$^3K_7 + {}^5G_4$	0.0058	0.0361	0.0697	386	0.1626	0.1960
$^3G_5$	0.0000	0.5338	0.0002	419	1.057	1.1136
$^5F_1 + {}^5G_6$	1.5201	0.8410	0.1411	451	2.1353	2.1508
$^3K_8$	0.0208	0.0334	0.1535	465	0.2210	0.3364
$^3F_2$	0.0000	0.0000	0.2041	475	0.3471	0.3518
$^3F_3$	0.0000	0.0000	0.3464	486	0.5128	0.5971
$^5F_4 + {}^5S_2$	0.0000	0.2392	0.9339	540	2.1258	2.1087
$^5F_5$	0.0000	0.4250	0.5687	644	1.9188	1.8667
$^5I_5$	0.0000	0.0100	0.0936	892	0.1368	0.1822

Table 6
Calculated branching ratios and lifetimes in Ho^{3+} YAG.

Transition	$\bar{\lambda}\,(nm)$	$S_{ED}\,(10^{-20}\,\mathrm{cm}^2)$	$A_{ED}\,(sec^{-1})$	$A_{MD}\,(sec^{-1})$	β	$\tau_r\,(ms)$	$\tau_m\,(ms)$
$^5F_2 \rightarrow {}^5F_3$	21645	0.005	0.00		0.0000		
$^5F_2 \rightarrow {}^5F_4$	3971	0.223	2.62		0.0004		
$^5F_2 \rightarrow {}^5S_2$	3785	0.007	0.10		0.0000		
$^5F_2 \rightarrow {}^5F_4$	1794	0.264	36.54		0.0060		
$^5F_2 \rightarrow {}^5I_4$	1293	0.136	51.01		0.0084		
$^5F_2 \rightarrow {}^5I_5$	1022	0.470	360.39		0.0596		
$^5F_2 \rightarrow {}^5I_6$	811	0.620	963.00		0.1592		
$^5F_2 \rightarrow {}^5I_7$	632	0.561	1870.88		0.3093		
$^5F_2 \rightarrow {}^5I_8$	479	0.352	2764.51		0.4570	0.165	
$^5F_3 \rightarrow {}^5F_4$	4864	0.238	1.03		0.0002		
$^5F_3 \rightarrow {}^5S_2$	4587	0.001	0.00		0.0000		
$^5F_3 \rightarrow {}^5F_5$	1956	1.355	103.05		0.0167		
$^5F_3 \rightarrow {}^5I_4$	1376	0.886	196.73		0.0318		
$^5F_3 \rightarrow {}^5I_5$	1073	0.483	228.55		0.0370		
$^5F_3 \rightarrow {}^5I_6$	842	0.561	554.52		0.0897		
$^5F_3 \rightarrow {}^5I_7$	651	0.907	1970.62		0.3189		
$^5F_3 \rightarrow {}^5I_8$	490	0.597	3124.06		0.5056	0.162	
$^5F_4 \rightarrow {}^5S_2$	80645	0.039	0.00		0.0013		
$^5F_4 \rightarrow {}^5F_5$	3271	0.226	2.72	5.03	0.0004		
$^5F_4 \rightarrow {}^5I_4$	1918	0.495	31.07		0.0051		
$^5F_4 \rightarrow {}^5I_5$	1376	1.077	185.72		0.0303		
$^5F_4 \rightarrow {}^5I_6$	1018	0.831	357.67		0.0584		
$^5F_4 \rightarrow {}^5I_7$	751	0.470	512.01		0.0836		
$^5F_4 \rightarrow {}^5I_8$	545	1.721	5028.27		0.8213	0.163	
$^5S_2 \rightarrow {}^5F_5$	3410	0.029	0.55		0.0001		
$^5S_2 \rightarrow {}^5I_4$	1965	0.540	56.72		0.0153		
$^5S_2 \rightarrow {}^5I_5$	1400	0.192	56.59		0.0153		
$^5S_2 \rightarrow {}^5I_6$	1032	0.309	230.10		0.0616		
$^5S_2 \rightarrow {}^5I_7$	758	0.706	1344.16		0.3630		
$^5S_2 \rightarrow {}^5I_8$	549	0.391	2014.74		0.5441	0.270	0.037
$^5F_5 \rightarrow {}^5I_4$	4636	0.019	0.06		0.0000		
$^5F_5 \rightarrow {}^5I_5$	2376	0.341	9.10		0.0028		
$^5F_5 \rightarrow {}^5I_6$	1479	1.115	126.42		0.0388		
$^5F_5 \rightarrow {}^5I_7$	975	1.438	577.68		0.1772		
$^5F_5 \rightarrow {}^5I_8$	654	1.872	2547.54		0.7813	0.307	0.004
$^5I_4 \rightarrow {}^5I_5$	4873	1.830	6.08	2.81	0.0632		
$^5I_4 \rightarrow {}^5I_6$	2172	1.203	51.63		0.3668		
$^5I_4 \rightarrow {}^5I_7$	1235	0.277	66.39		0.4716		
$^5I_4 \rightarrow {}^5I_8$	762	0.013	13.85		0.0984	7.10	
$^5I_5 \rightarrow {}^5I_6$	3919	1.348	7.49	6.81	0.0611		
$^5I_5 \rightarrow {}^5I_7$	1655	1.579	127.25		0.5437		
$^5I_5 \rightarrow {}^5I_8$	903	0.182	92.48		0.3952	4.27	0.006
$^5I_6 \rightarrow {}^5I_7$	2865	1.886	23.85	16.84	0.1415		
$^5I_6 \rightarrow {}^5I_8$	1173	1.273	246.82		0.8585	3.48	0.045
$^5I_7 \rightarrow {}^5I_8$	1988	2.906	98.15	29.78	1.0000	7.82	7.00

Table 7
Measured and calculated values for the Linestrength in Ho^{3+} LuAG.

Transition (from $^5I_8$)	$\mid \langle U^{(2)} \rangle \mid^2$	$\mid \langle U^{(4)} \rangle \mid^2$	$\mid \langle U^{(6)} \rangle \mid^2$	$\bar{\lambda}$(nm)	Linestrength(10^{-20} cm^2)	
					measured	calculated
$^3K_6 + {}^3F_4$	0.0026	0.1263	0.0073	324	0.2791	0.2631
$^3L_9 + {}^5G_3$	0.0185	0.0052	0.1169	346	0.2115	0.2891
$^3D_2 + {}^3H_6 + {}^5G_5$	0.2155	0.1969	0.1679	362	0.7842	0.6962
$^3K_7 + {}^5G_4$	0.0058	0.0361	0.0697	387	0.2160	0.1879
$^3G_5$	0.0000	0.5338	0.0002	419	1.0673	1.0609
$^5F_1 + {}^5G_6$	1.5201	0.8410	0.1411	450	2.0842	2.0943
$^3K_8$	0.0208	0.0334	0.1535	465	0.2019	0.3232
$^3F_2$	0.0000	0.0000	0.2041	474	0.3491	0.3380
$^3F_3$	0.0000	0.0000	0.3464	486	0.5120	0.5737
$^5F_4 + {}^5S_2$	0.0000	0.2392	0.9339	541	2.1061	2.0220
$^5F_5$	0.0000	0.4250	0.5687	644	1.7139	1.7863
$^5I_5$	0.0000	0.0100	0.0936	898	0.1524	0.1749

Table 8
Calculated branching ratios and lifetimes in Ho^{3+} LuAG.

Transition	$\bar{\lambda}\,(nm)$	$S_{ED}\,(\mathbf{10^{-20}\,cm^2})$	$A_{ED}\,(sec^{-1})$	$A_{MD}\,(sec^{-1})$	β	$\tau_r\,(ms)$	$\tau_m\,(ms)$
$^5F_2 \rightarrow {}^5F_3$	28248	0.006	0.30		0.0001		
$^5F_2 \rightarrow {}^5F_4$	4162	0.213	2.20		0.0004		
$^5F_2 \rightarrow {}^5S_2$	3957	0.007	0.09		0.0000		
$^5F_2 \rightarrow {}^5F_4$	1832	0.253	33.53		0.0058		
$^5F_2 \rightarrow {}^5I_4$	1313	0.131	47.65		0.0083		
$^5F_2 \rightarrow {}^5I_5$	1035	0.448	337.15		0.0585		
$^5F_2 \rightarrow {}^5I_6$	819	0.595	913.56		0.1584		
$^5F_2 \rightarrow {}^5I_7$	637	0.537	1779.62		0.3085		
$^5F_2 \rightarrow {}^5I_8$	482	0.338	2653.86		0.4601	0.173	
$^5F_3 \rightarrow {}^5F_4$	4880	0.231	1.01		0.0002		
$^5F_3 \rightarrow {}^5S_2$	4602	0.001	0.00		0.0000		
$^5F_3 \rightarrow {}^5F_5$	1959	1.302	100.35		0.0167		
$^5F_3 \rightarrow {}^5I_4$	1377	0.849	191.40		0.0318		
$^5F_3 \rightarrow {}^5I_5$	1074	0.461	221.04		0.0367		
$^5F_3 \rightarrow {}^5I_6$	843	0.538	539.53		0.0897		
$^5F_3 \rightarrow {}^5I_7$	651	0.867	1913.42		0.3181		
$^5F_3 \rightarrow {}^5I_8$	491	0.574	3048.32		0.5068	0.166	
$^5F_4 \rightarrow {}^5S_2$	80645	0.037	0.00		0.0013		
$^5F_4 \rightarrow {}^5F_5$	3273	0.221	2.71	5.03	0.0005		
$^5F_4 \rightarrow {}^5I_4$	1919	0.475	30.34		0.0051		
$^5F_4 \rightarrow {}^5I_5$	1377	1.032	181.04		0.0304		
$^5F_4 \rightarrow {}^5I_6$	1019	0.794	347.69		0.0583		
$^5F_4 \rightarrow {}^5I_7$	752	0.449	496.51		0.0833		
$^5F_4 \rightarrow {}^5I_8$	545	1.650	4900.16		0.8217	0.168	
$^5S_2 \rightarrow {}^5F_5$	3412	0.028	0.54		0.0001		
$^5S_2 \rightarrow {}^5I_4$	1966	0.519	55.39		0.0153		
$^5S_2 \rightarrow {}^5I_5$	1401	0.184	55.25		0.0153		
$^5S_2 \rightarrow {}^5I_6$	1032	0.296	224.64		0.0621		
$^5S_2 \rightarrow {}^5I_7$	759	0.678	1313.27		0.3630		
$^5S_2 \rightarrow {}^5I_8$	549	0.376	1968.28		0.5441	0.276	0.031
$^5F_5 \rightarrow {}^5I_4$	4638	0.018	0.06		0.0000		
$^5F_5 \rightarrow {}^5I_5$	2378	0.328	8.89		0.0028		
$^5F_5 \rightarrow {}^5I_6$	1480	1.070	123.45		0.0388		
$^5F_5 \rightarrow {}^5I_7$	976	1.376	562.56		0.1772		
$^5F_5 \rightarrow {}^5I_8$	654	1.791	2479.97		0.7811	0.315	0.003
$^5I_4 \rightarrow {}^5I_5$	4878	1.757	5.97	2.81	0.0673		
$^5I_4 \rightarrow {}^5I_6$	2173	1.156	50.52		0.3668		
$^5I_4 \rightarrow {}^5I_7$	1236	0.266	64.90		0.4712		
$^5I_4 \rightarrow {}^5I_8$	762	0.013	13.54		0.0983	7.26	
$^5I_5 \rightarrow {}^5I_6$	3917	1.293	7.35	7.35	0.0640		
$^5I_5 \rightarrow {}^5I_7$	1655	1.517	124.49		0.5423		
$^5I_5 \rightarrow {}^5I_8$	903	0.175	90.38		0.3937	4.35	0.004
$^5I_6 \rightarrow {}^5I_7$	2866	1.811	23.85	17.12	0.1424		
$^5I_6 \rightarrow {}^5I_8$	1174	1.223	246.82		0.8576	3.47	0.040
$^5I_7 \rightarrow {}^5I_8$	1988	2.790	98.15	30.27	1.0000	7.79	7.10

Table 9
Judd-Ofelt intensity parameters, Ω_λ, and RMS deviation, δ, for Ho:YAG and Ho:LuAG.

ion:host	$\Omega_2(\text{x}10^{-20}\,\text{cm}^2)$	$\Omega_2(\text{x}10^{-20}\,\text{cm}^2)$	$\Omega_2(\text{x}10^{-20}\,\text{cm}^2)$	$\delta(\text{x}10^{-20}\,\text{cm}^2)$	reference
Ho:YAG	0.101 ± 0.087	2.086 ± 0.097	1.724 ± 0.064	0.071	this study
Ho:LuAG	0.125 ± 0.087	1.987 ± 0.097	1.656 ± 0.064	0.108	this study
Ho:YAG	0.04	2.67	1.89	0.089	[22]
Ho:LuAG	0.172 ± 0.10	2.08 ± 0.18	1.92 ± 0.11	–	[23]

Fig. 1. Cross section versus temperature for spectral lines at 1847.7 and 1853.6 nm in $^5I_8 \rightarrow {}^5I_7$ Ho:YAG absorption.

Fig. 2. Temperature dependence of Ho $^5I_7$ absorption in YAG from 10-100K.

Fig. 3. Temperature dependence of the Ho $^5I_7$ absorption in YAG from 125-295K.

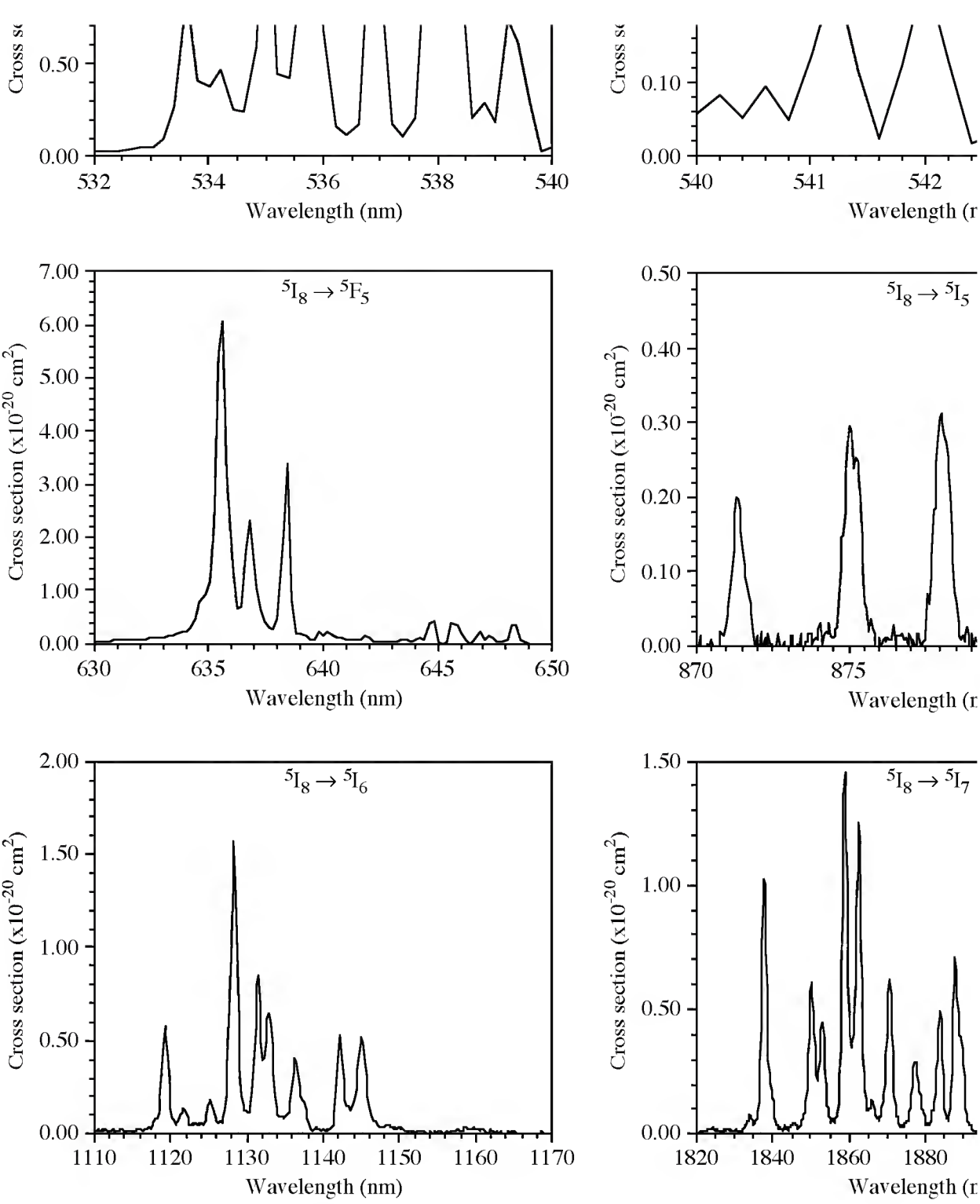

Fig. 4. Absorption spectra of Ho:LuAG at 10K

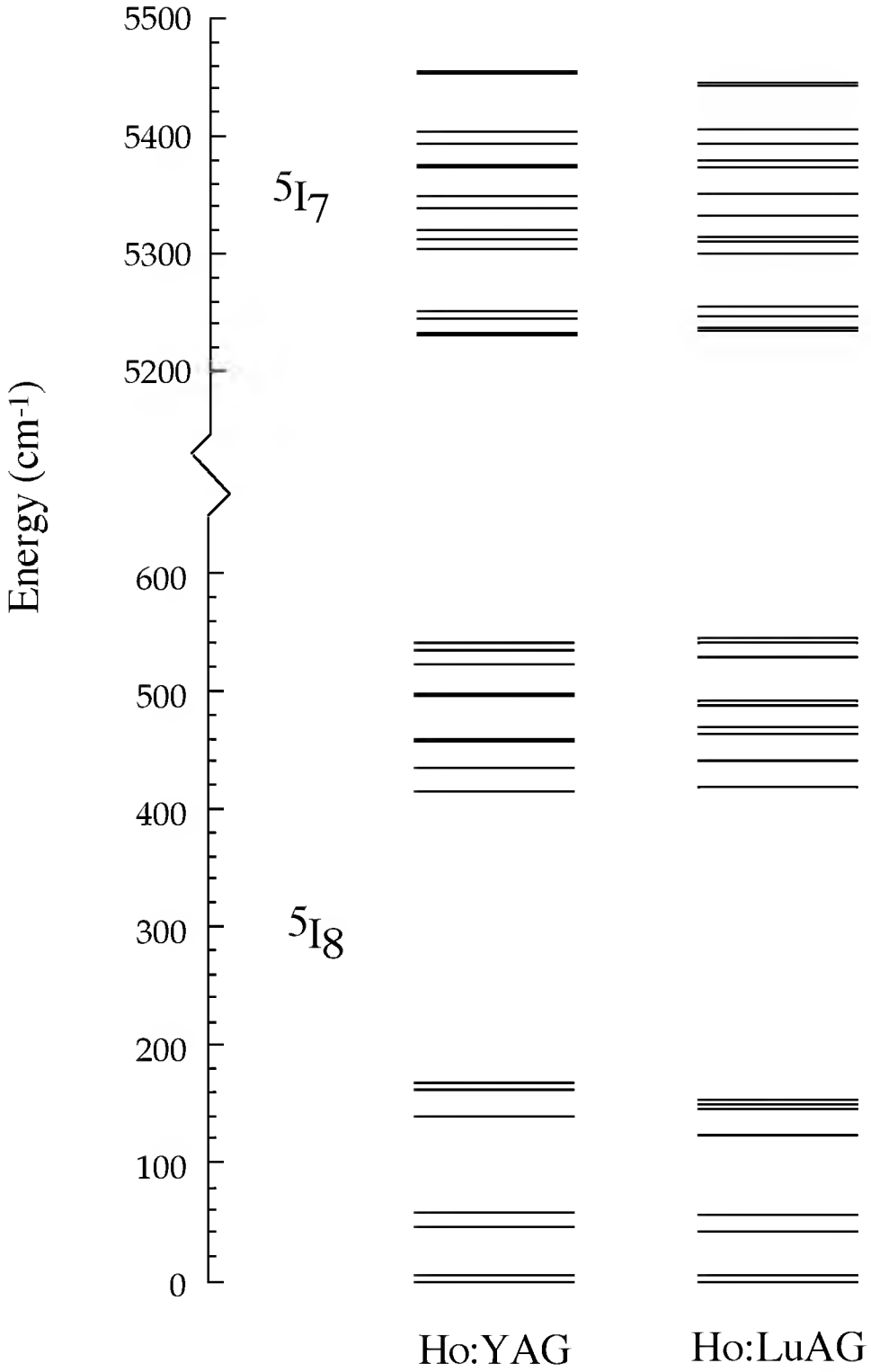

Fig. 5. Theoretical energy levels of the two lowest manifolds in Ho:YAG and Ho:LuAG.